24th COBEM - 2017

24th ABCM International Congress of Mechanical Engineering
December 3-8, 2017, Curitiba, PR, Brazil

COBEM-2017-0045
AEROELASTIC MODELING OF LOW SPEED PITCHING OSCILLATIONS INDUCED BY STALL CONSIDERING NONLINEAR SPRINGS

Carlos Renan dos Santos
Flávio Donizeti Marques
Universidade de São Paulo, Escola de Engenharia de São Carlos, SP, Brazil
carlos.renan.santos@usp.br, fmarques@sc.usp.br

Abstract. *Beyond the flutter velocity, a nonlinear aeroelastic system can oscillate in a limit cycle condition. With vibrations reaching higher angles of attack, nonlinear aerodynamic effects like dynamic stall become relevant and dominant. The modeling of structural and aerodynamic effects during stall-induced oscillations is crucial for understanding the phenomenon. In this sense, the present work proposes an investigation on the influence of structural nonlinearities on the aeroelastic behavior of a pitching airfoil. A computational model which couples the equation of motion for a typical section with the Beddoes-Leishman model for unsteady aerodynamics is employed. The model is validated and the behavior of the system is analyzed by considering a pitch spring with stiffness represented by hardening, softening, and freeplay nonlinear effects. It was concluded that structural stiffness can affect the flutter onset velocity and the behavior of the stall-induced oscillations as the airspeed varies.*

Keywords: *Nonlinear aeroelasticity, Beddoes-Leishman model, Dynamic stall, Stall-induced oscillations (SIO), Stall flutter.*

1. INTRODUCTION

Stall-induced oscillations (SIO) consist of a nonlinear aeroelastic behavior that may occur when a system reaches stall conditions during dynamic motions. According to aerodynamic and structural properties, the vibrations can have a limit cycle shape as an effect of the dynamic stall. In these cases, aerodynamic loads are influenced by some events observed in the flow past the airfoil, such as the vortex shedding from the leading edge, the separation of the flow from the airfoil trailing edge or the delay observed between the angle of attack when the flow separates from the aerodynamic surface and the angle when reattachment occurs (McCroskey, 1981).

Helicopter rotors or blades of wind turbines are examples of aeroelastic systems where SIO can be observed (Conlisk, 1997; Leishman, 2002; Hansen, 2015). However, vibrations can reduce the performance and the fatigue life of the machines where they occur. This problem has motivated the research on aerodynamic models able to capture dynamic stall features. To avoid high computational costs, commonly associated with analysis based on computational fluid dynamics (CFD), the helicopter industry has developed semi-empirical approaches, such as the Beddoes-Leishman (Leishman and Beddoes, 1986) and the ONERA (Petot, 1989) models. These models require the adjustment of certain empirical constants extracted from airfoil data.

Recently, SIO have been investigated as a key to the development of energy harvesters (Chen *et al.*, 2014; Onoue *et al.*, 2015). When considering the operational regime for such harvesters not only high Mach numbers need to be taken into account but also low wind speeds. Some work has been developed in order to apply the Beddoes-Leishman model to the modeling of low speed prescribed oscillations (Sheng *et al.*, 2006) or to the analysis of SIO by considering a linear structural stiffness for plunge and pitch motions (Song *et al.*, 2011).

From the viewpoint of structural modeling, typical aeroelastic sections are usually employed in two-dimensional analysis (Bichiou *et al.*, 2016; Sarkar and Bijl, 2008). On the other hand, nonlinearities related to structural effects need to be taken into account. Hardening, softening, freeplay or hysteresis from the stiffness behavior can influence the flutter onset velocity, the amplitudes and the frequencies of oscillations (Marques *et al.*, 2015).

In this sense, the present work proposes the modeling of SIO at low wind speeds by considering one degree of freedom and accounting for the effects of different nonlinear torsional springs. The computational model is based on the equation of motion for a pitching typical aeroelastic section with aerodynamic coefficients given by the Beddoes-Leishman model in state space representation.

2. METHODOLOGY

Aeroelastic analysis for SIO with one degree of freedom is based on the solution of the equation of motion for a pitching airfoil, that is:

$$I_\alpha \ddot{\alpha} + K_\alpha F(\alpha) = M_{ea} \ , \tag{1}$$

where I_α denotes the moment of inertia of the system in relation to the elastic axis, α is the instantaneous angle of attack, $F(\alpha)$ is a function describing how the torsional stiffness varies with the angle of attack and $M_{ea}(t)$ is the aerodynamic moment in relation to the elastic axis at each instant of time t.

Dimensionless parameters can be adopted being the mass ratio $\mu = 4m/(\pi\rho c^2)$, where ρ is the air density, c is the airfoil chord length and m is its mass; the radius of gyration $r_\alpha^2 = 4I_\alpha/(mc^2)$; the natural frequency of pitching $\omega_\alpha = \sqrt{K_\alpha/I_\alpha}$ and the aerodynamic moment coefficient at the elastic axis $C_{m_{ea}} = 2M_{ea}/(\rho V^2 c^2)$, where V is the freestream velocity. By doing so, Eq. (1) becomes:

$$\ddot{\alpha} + \omega_\alpha^2 F(\alpha) = \frac{8V^2 C_{m_{ea}}}{\pi\mu r_\alpha^2 c^2} \tag{2}$$

The aerodynamic coefficient is given for each instant through the Beddoes-Leishman model in state space formulation, which uses eight states to represent the attached flow condition:

$$\{\dot{x}\} = [A]\{x\} + [B]\begin{Bmatrix}\alpha \\ q\end{Bmatrix} \ , \tag{3}$$

$$\begin{Bmatrix}C_n^p \\ C_m^p\end{Bmatrix} = [C]\{x\} + [D]\begin{Bmatrix}\alpha \\ q\end{Bmatrix} \ , \tag{4}$$

where C_n^p and C_m^p are the coefficients for normal force and aerodynamic moment at the quarter chord, respectively, under fully attached flow. $\{x\}$ is the vector with the aerodynamic states, $[A]$ is a diagonal state matrix, $[B]$ is the input matrix, $[C]$ is the output matrix and $[D]$ is the feedthrough matrix. Such matrices are known from the scientific literature (Leishman and Crouse, 1989; Chantharasenawong, 2007; dos Santos *et al.*, 2017).

Moreover, other four states are defined to contribute to the resultant loads by expressing mathematically the physical phenomena associated with the dynamic stall behavior: one state is related to the delay in the normal force in relation to that expected linearly; two states are associated with the leading edge flow separation; and one state models the vortex shedding from the leading edge.

The lag on the normal force coefficient is modeled in a state space representation with the dependence on a time constant T_p:

$$\dot{x}_9 = \left(\frac{2V}{c}\right)\frac{-x_9 + C_n^p}{T_P} \ , \tag{5}$$

$$C_n^*(t) = x_9 \ . \tag{6}$$

Under stationary conditions, Leishman and Beddoes (1989) presented an empirical approach to determine the fraction f of the airfoil where the flow is attached, that is:

$$f(\hat{\alpha}) = \begin{cases} 1 - 0.3e^{\frac{|\hat{\alpha}| - \alpha_1}{s_1}} & \text{se } |\hat{\alpha}| \leq \alpha_1 \\ 0.04 - 0.66e^{\frac{\alpha_1 - |\hat{\alpha}|}{s_2}} & \text{se } |\hat{\alpha}| > \alpha_1 \end{cases} \ , \tag{7}$$

where α_1 is an angle defined when $f = 0.7$, s_1 and s_2 are empirical constants and $\hat{\alpha}$ is a dummy variable to represent a generic angle.

Dynamically, the flow separation from the leading edge is also delayed in relation to the stationary condition. The state x_{10} calculates the lagged separation point as function of an effective angle of attack given by the delayed normal force coefficient according to:

$$\dot{x}_{10} = \left(\frac{2V}{c}\right)\frac{-x_{10} + f\left(\frac{C_n^*}{C_{n_\alpha}}\right)}{T_f} \ , \tag{8}$$

$$f_1(t) = x_{10} \ , \tag{9}$$

where T_f is a empirical time constant and C_{n_α} is the slope of the curve for normal force coefficient per angle of attack under stationary conditions.

The delayed normal force coefficient is also used to trigger the vortex shedding phase. The model considers that this phase starts when $|C_n^*(t)| \geq C_{n_1}$, with C_{n_1} being the value of C_n at the eminence of stall under stationary conditions. Therefore, a dimensionless counter τ_v is established and increases with the dimensionless time $2Vt/c$. In state space representation the normal force coefficient due to the vortex shedding phase is given by:

$$\dot{x}_{11} = \left(\frac{2V}{c}\right) \frac{-x_{11} + \dot{C}_v}{T_v} \ , \tag{10}$$

$$C_n^v(t) = x_{11} \ , \tag{11}$$

where T_v is a time constant and:

$$C_v = \begin{cases} C_n^c[1 - 0.25(1 + \sqrt{f_1})^2] & \text{, if } \tau_v \leq 2T_{vl} \\ 0 & \text{, if } \tau_v > 2T_{vl} \ , \end{cases} \tag{12}$$

with T_{vl} being an empirical time constant defined as the dimensionless time needed to the vortex to travel from the airfoil leading edge to its trailing edge.

Such phenomenon also influences the moment coefficient at the quarter chord according to the empirical representation:

$$C_m^v(t) = -0.25 \left[1 - \cos\left(\frac{\pi\tau_v}{T_{vl}}\right)\right] C_n^v \ . \tag{13}$$

During the vortex shedding phase the parameters T_f, T_v and α_1 are modified for a better representation of the dynamic stall (Chantharasenawong, 2007; dos Santos *et al.*, 2017):

$$T_f = \begin{cases} T_{f_0} & \text{if } 0 \leq \tau_v \leq T_{vl} \text{ and } \alpha\dot{\alpha} \geq 0 \\ \frac{1}{3}T_{f_0} & \text{if } T_{vl} < \tau_v \leq 2T_{vl} \text{ and } \alpha\dot{\alpha} \geq 0 \\ \frac{1}{2}T_{f_0} & \text{if } 0 \leq \tau_v \leq 2T_{vl} \text{ and } \alpha\dot{\alpha} < 0 \\ 4T_{f_0} & \text{if } 2T_{vl} < \tau_v \end{cases} , \tag{14}$$

$$T_v = \begin{cases} T_{v_0} & \text{if } 0 \leq \tau_v \leq T_{vl} \text{ and } \alpha\dot{\alpha} \geq 0 \\ 0.25T_{v_0} & \text{if } T_{vl} < \tau_v \leq 2T_{vl} \text{ and } \alpha\dot{\alpha} \geq 0 \\ 0.5T_{v_0} & \text{if } 0 \leq \tau_v \leq 2T_{vl} \text{ and } \alpha\dot{\alpha} < 0 \\ 0.9T_{v_0} & \text{if } 2T_{vl} < \tau_v \end{cases} , \tag{15}$$

$$\alpha_1 = \begin{cases} \alpha_{1_0} & \text{if } \alpha\dot{\alpha} \geq 0 \\ \alpha_{1_0} - [1 - f_a(t)]^{0.25}\delta_{\alpha_1} & \text{if } \alpha\dot{\alpha} < 0 \end{cases} , \tag{16}$$

where the subscript 0 denotes the value of each parameter before the vortex shedding and δ_{α_1} is the maximum reduction in α_1 during this phase.

The reattachment phase is triggered when $|C_n'(t)| < C_{n_1}$ and $|\alpha(t)|$ is decreasing. From this moment, $\alpha_1 = \alpha_{1_0}$, $T_v = T_{v_0}$, and T_f is given by:

$$T_f = \begin{cases} T_{f_0} & \text{if } f_a(t) \geq 0.7 \\ 2T_{f_0} & \text{if } f_a(t) < 0.7 \end{cases} . \tag{17}$$

Another state related to the flow separation is required for a better representation of the dynamic stall. Such state considers the instantaneous angle of attack according to the state space representation:

$$\dot{x}_{12} = \left(\frac{2V}{c}\right) \frac{-2x_{12} + 2f(\alpha)}{T_{f_0}} \ , \tag{18}$$

$$f_2(t) = x_{12} \ . \tag{19}$$

If a parameter $\hat{f}$ is defined as $\hat{f} = \max[f_1(t), f_2(t)]$, the parcels of aerodynamic coefficients due to the flow separation from the trailing edge are given by:

$$\begin{cases} C_n^f(t) = C_n^c(t) \left(\frac{1+\sqrt{f_1}}{2}\right)^2 \\ C_m^f(t) = \left\{K_0 + K_1(1 - \hat{f}) + K_2 \sin[\pi(\hat{f})^m]\right\} C_n^c(t) + C_{m_0} \end{cases} , \tag{20}$$

where $m = 2$, K_0, K_1 and K_2 are empirical constants that match the moment coefficient per angle of attack under stationary conditions, C_{m_0} is the value of the moment coefficient in the absence of normal force and $C_n^c(t)$ is the circulatory component of the normal force.

Summing up the contributions for each flow event during unsteady motions, the normal force coefficient results in: $C_n(t) = C_n^p(t) - C_n^c(t) + C_n^f(t) + C_n^v(t)$ and the aerodynamic moment coefficient at the quarter chord is given by: $C_m(t) = C_m^p(t) + C_m^f(t) + C_m^v(t)$. At the elastic axis, the aerodynamic moment is such that:

$$C_{m_{ea}}(t) = C_m(t) + C_n(t)(x_{ea} - x_{ca}) \ , \tag{21}$$

where x_{ea} is the percentage of the chord length where the elastic axis is located and x_{ca} is the position of the aerodynamic center, here taken as 0.25.

Values for all empirical parameters in the Beddoes-Leishman model can be found in the literature for the NACA 0012 airfoil (Leishman and Beddoes, 1986; dos Santos *et al.*, 2017).

3. RESULTS AND DISCUSSIONS

The aeroelastic model was validated by comparing its results with those found in the scientific literature (Vasconcellos *et al.*, 2016). The analyzed system consists of a NACA 0012 airfoil with a chord length of $0.265\ m$ and elastic axis at 34% of the chord length. The restoring moment from the spring was considered as $K_\alpha F(\alpha) = 6.58\alpha^3 + 1.65\alpha\ (Nm)$ and the parameter $r_\alpha^2\mu = 5.14$. Figure 1(a) shows the Hopf bifurcation for computational and experimental results. A good agreement between the values predicted by the model and those measured in the wind tunnel test can be observed. Minor differences are observed between 11 – 12 m/s which can be explained by effects of dynamic damping that were not taken into account in the model. In special, near to 12 m/s, there is a transition from non-symmetrical to symmetrical oscillations around the $\alpha = 0°$–axis according to experimental results. Computationally, the same behavior is observed near to 11 m/s. Figure 1(b) makes clear the change of non-symmetrical to symmetrical oscillations around $\alpha = 0°$ by analyzing the mean angle of vibration and the total amplitude of motion (from maximum to minimum angle of attack). Another jump in SIO amplitudes is observed near to 12 m/s.

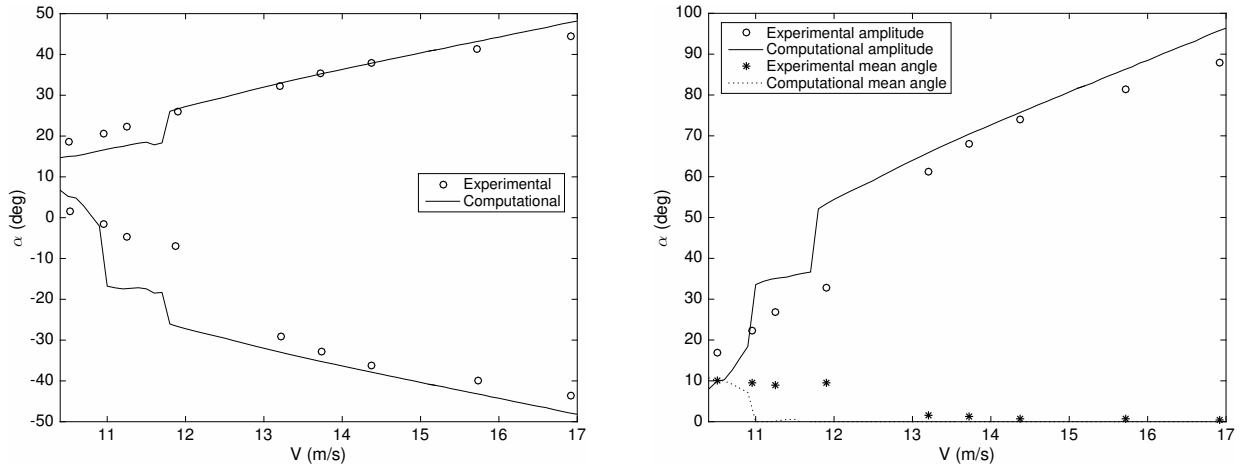

(a) Hopf bifurcation

(b) Peak-to-peak analysis

Figure 1. Comparison of the computational model with experimental results.

With the model validated, different nonlinear springs were selected for SIO analyses. The simulations adopted a system with an airfoil NACA 0012 with chord length of $0.25\ m$, elastic axis at 30% of the chord length, $\omega_\alpha = 1.8\ Hz$ and $r_\alpha^2\mu = 5$. A linear stiffness with $F(\alpha) = \alpha$, a hardening stiffness with $F(\alpha) = 0.2\alpha^3 + \alpha$, a softening spring with $F(\alpha) = -0.1\alpha^3 + \alpha$ and three different freeplay stiffness were considered. The freeplay nonlinearity is associated with the function (Vasconcellos *et al.*, 2012):

$$F(\alpha) = 0.5\left\{1 - \tanh[\epsilon(\alpha + \delta)]\right\}(\alpha + \delta) + 0.5\left\{1 + \tanh[\epsilon(\alpha - \delta)]\right\}(\alpha - \delta) \ , \tag{22}$$

where δ denotes the freeplay boundary region, and ϵ determines the smoothness of the function, here chosen as 10000.

Figure 2(a) considers $\delta = 5°$ to illustrate the function $F(\alpha)$ which represents freeplay stiffness and Fig. 2(b) indicates $F(\alpha)$ for hardening and softening nonlinearities compared with the function $F(\alpha)$ in the linear case. Figure 3 shows Hopf bifurcations by considering the different springs. The Hopf bifurcation indicates the maximum and the minimum values of α during limit cycle oscillations. It can be observed that the linear and the cubic springs impose the same flutter onset velocity to the system when limit cycle oscillations begin. However, the freeplay nonlinearity reduces the flutter

velocity and before the flutter onset the angle where the system reaches its equilibrium increases as the freestream velocity increases.

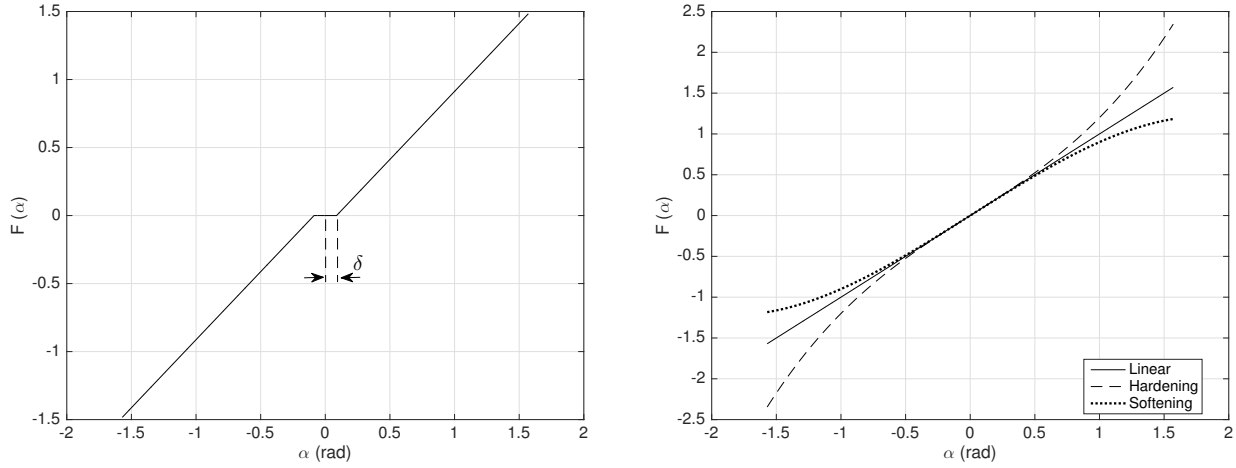

(a) Freeplay nonlinearities (b) Cubic nonlinearities

Figure 2. Characterization of the nonlinear springs.

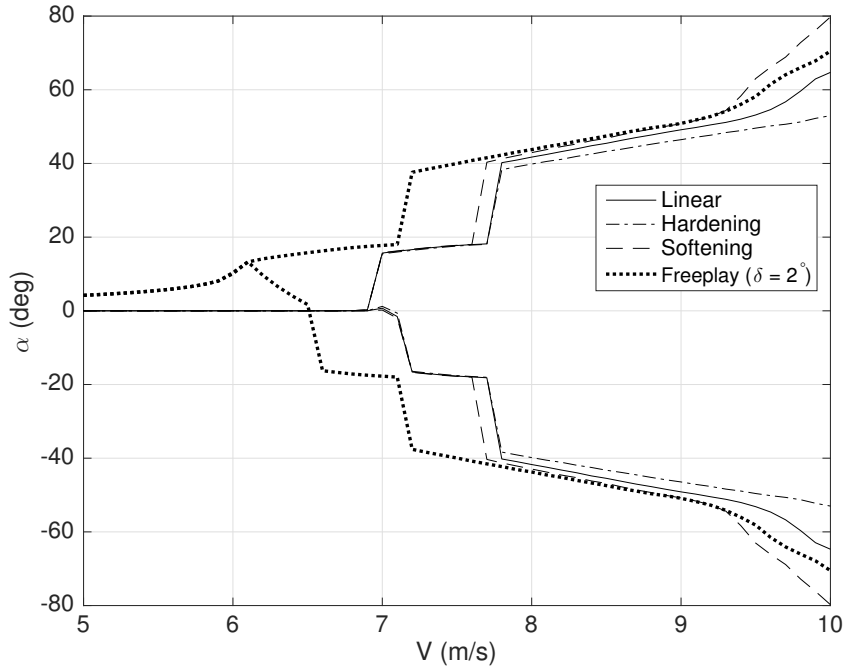

Figure 3. Hopf bifurcations for different nonlinear springs.

Two jumps in amplitudes can be observed. The first usually occurs at the frontier between symmetrical and asymmetrical oscillations around $\alpha = 0°$. The second jump occurs when the amplitude of oscillation reaches about 20°. Physical events associated with such behavior can be investigated by analyzing phase portraits of the motions. Figure 4 shows the phase portraits in four wind speeds for the different springs analyzed in Fig. 3. The freestream velocity of 6.5 m/s defines the frontier between symmetrical and asymmetrical oscillations around $\alpha = 0°$ for the system with a freeplay spring. At this velocity, the systems with other springs have damped oscillations. At the wind speed of 7.1 m/s, there is the second jump in amplitudes for the system with freeplay stiffness and the first jump for other springs. When comparing the phase portraits for the velocities of 7.1 and 7.7 m/s it is clear that the systems had enough energy to modify their oscillatory behavior. By observing the phase portrait for $V = 7.7\ m/s$ one can conclude that linear and hardening springs impose restoring moments able to retard the second jump of the system. On the other hand, the systems with softening and freeplay nonlinearities had energy enough to increase their amplitudes of oscillation. This fact reinforces the relevance of structural nonlinearities on SIO. At $V = 10\ m/s$, all systems have similar phase portraits. Differences in the amplitudes of oscillation are related to the restoring moment that each spring imposes to the system at high angles of attack.

It can be observed that the freeplay nonlinearity anticipates the motion observed for other springs at higher wind

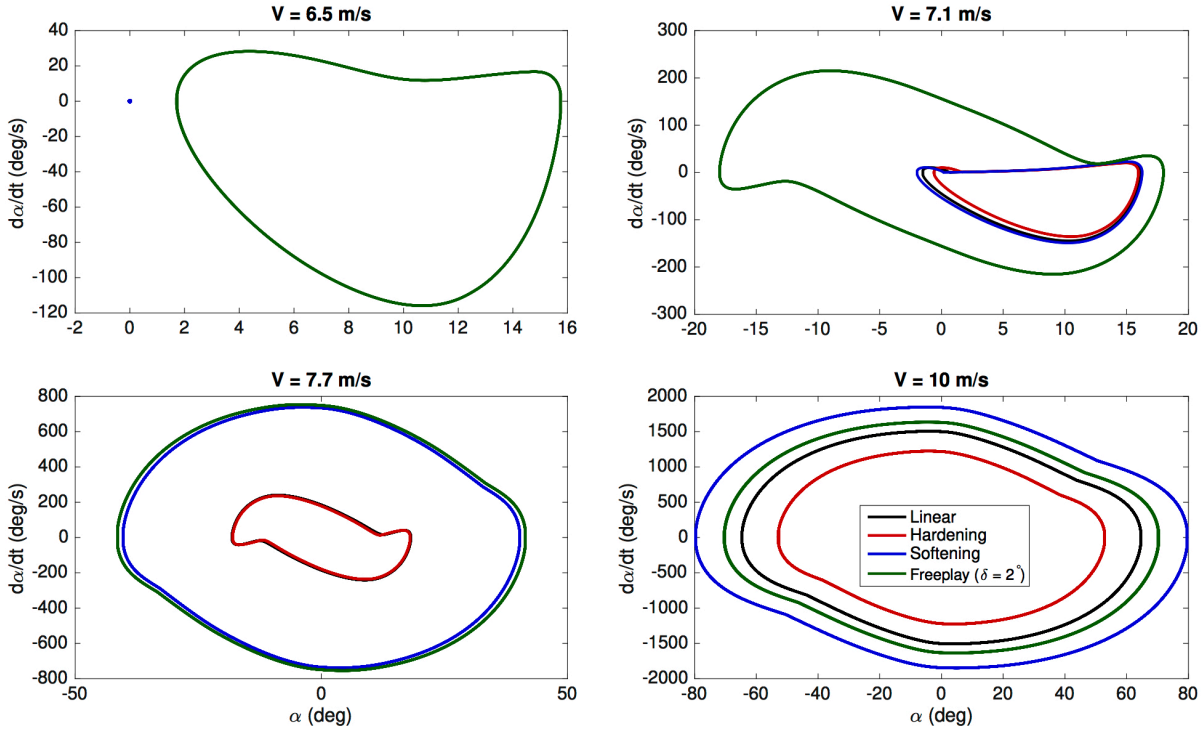

Figure 4. Phase portraits for different freestream velocities and springs.

speeds. Such behavior can be associated with the lower stiffness during the freeplay boundary region. To investigate this hypothesis, different freeplay springs were analyzed by varying the value of δ. Figure 5 presents the Hopf bifurcations for δ values of 1°, 2° and 5°. It is observed that the flutter velocity decreases as the freeplay boundary region increases. Moreover, the equilibrium position before the flutter onset reaches higher angles as the value of δ increases and higher amplitudes of motion are attained which confirms the influence of the freeplay boundary region on the SIO behavior.

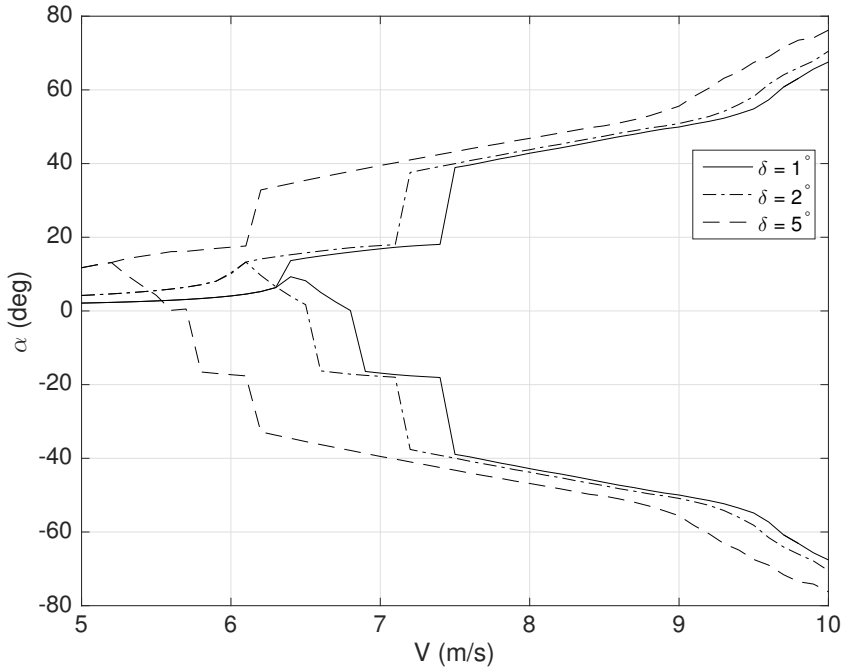

Figure 5. Hopf bifurcations for different pitch springs with freeplay.

4. CONCLUSIONS

The present work uses an aeroelastic model based on the equation of motion for a pitching typical section coupled to the Beddoes-Leishman model for unsteady aerodynamics, which considers dynamic stall effects at high angles of attack. The model was validated by comparing computational results with experimental data and analyses of stall-induced oscillations were performed by considering different nonlinear springs. It was observed that structural nonlinearities can influence the amplitude of the oscillations and the wind speeds where these amplitudes suddenly change. Most significant influences of structural properties on the aeroelastic behavior of the system are related to the freeplay nonlinearity which reduces the flutter velocity and the equilibrium position of the system before the flutter onset. In conclusion, structural nonlinearities are determinant on the behavior of stall-induced oscillations.

5. ACKNOWLEDGEMENTS

This work was supported by grants #2016/24522-4, #2017/09468-6 and #2017/02926-9, São Paulo Research Foundation (FAPESP) and grant #307658/2016-3, National Council for Scientific and Technological Development (CNPq).

6. REFERENCES

Bichiou, Y., Nuhait, A.O., Abdelkefi, A. and Hajj, M.R., 2016. "Unsteady aeroelastic behaviors of rigid airfoils with preset angles of attack". *Journal of Vibration and Control*, Vol. 22, No. 4, pp. 1010–1022.

Chantharasenawong, C., 2007. *Nonlinear aeroelastic behaviour of aerofoils under dynamic stall*. Ph.D. thesis, University of London, London.

Chen, J., Dhanushkodi, A. and Lee, C.L., 2014. "Energy harvesting measurements from stall flutter limit cycle oscillations". In *Active and Passive Smart Structures and Integrated Systems 2014*. San Diego, California, USA.

Conlisk, A.T., 1997. "Modern helicopter aerodynamics". *Annual review of fluid mechanics*, Vol. 29, No. 1, pp. 515–567.

dos Santos, C.R., Pereira, D.A. and Marques, F.D., 2017. "On limit cycle oscillations of typical aeroelastic section with different preset angles of incidence at low airspeeds". *Journal of Fluids and Structures*, Vol. 74, pp. 19–34.

Hansen, M.O.L., 2015. *Aerodynamics of wind turbines*. Routledge, Abingdon.

Leishman, J.G., 2002. "Challenges in modeling the unsteady aerodynamics of wind turbines". In *ASME 2002 Wind Energy Symposium*. Reno, Nevada, USA.

Leishman, J.G. and Beddoes, T.S., 1986. "A generalised model for aircraft unsteady aerodynamic behaviour and dynamic stall using the indicial method". In *42^{nd} Annual Forum of the American Helicopter Society*. Washington, DC, USA.

Leishman, J.G. and Beddoes, T.S., 1989. "A semi-empirical model for dynamic stall". *Journal of the American Helicopter Society*, Vol. 34, No. 3, pp. 3–17.

Leishman, J.G. and Crouse, G.L., 1989. "State-space model for unsteady airfoil behavior and dynamic stall". In *30^{th} Structures, Structural Dynamics and Materials Conference, Structures, Structural Dynamics, and Materials and Co-located Conferences*. Mobile, Alabama, USA.

Marques, F.D., Pereira, D.A. and Vasconcellos, R.M., 2015. "Nonlinear airfoil torsional response induced by separated flows". In *56^{th} AIAA/ASCE/AHS/ASC Structures, Structural Dynamics, and Materials Conference, AIAA SciTech Forum*. Kissimmee, Florida, USA.

McCroskey, W.J., 1981. "The phenomenon of dynamic stall". Technical report, NASA and US Army Aviation Research and Development Command, Moffett Field, USA.

Onoue, K., Song, A., Strom, B. and Breuer, K.S., 2015. "Large amplitude flow-induced oscillations and energy harvesting using a cyber-physical pitching plate". *Journal of Fluids and Structures*, Vol. 55, pp. 262–275.

Petot, D., 1989. "Differential equation modeling of dynamic stall". *Recherche Aérospatiale*, , No. 5, pp. 59–72.

Sarkar, S. and Bijl, H., 2008. "Nonlinear aeroelastic behavior of an oscillating airfoil during stall-induced vibration". *Journal of Fluids and Structures*, Vol. 24, No. 6, pp. 757–777.

Sheng, W., Galbraith, R.A.M. and Coton, F.N., 2006. "A new stall-onset criterion for low speed dynamic-stall". *Journal of Solar Energy Engineering*, Vol. 128, No. 4, pp. 461–471.

Song, S., Qinghua, Z., Zhang, C. and Xianping, N., 2011. "Airfoil aeroelastic flutter analysis based on modified Leishman-Beddoes model at low Mach number". *Chinese Journal of Aeronautics*, Vol. 24, No. 5, pp. 550–557.

Vasconcellos, R.M.G., Abdelkefi, A., Marques, F.D. and Hajj, M.R., 2012. "Representation and analysis of control surface freeplay nonlinearity". *Journal of Fluids and Structures*, Vol. 31, pp. 79–91.

Vasconcellos, R.M.G., Pereira, D.A. and Marques, F.D., 2016. "Characterization of nonlinear behavior of an airfoil under stall-induced pitching oscillations". *Journal of Sound and Vibration*, Vol. 372, pp. 283–298.

7. RESPONSIBILITY NOTICE

The authors are the only responsible for the printed material included in this paper.